

Towards Trustworthy Selective Generation: Reliability-Guided Diffusion for Ultra-Low-Field to High-Field MRI Synthesis

Zhenxuan Zhang¹, Peiyuan Jing¹, Ruicheng Yuan¹, Liwei Hu¹, Anbang Wang¹,
Fanwen Wang¹, Yinzhe Wu¹, Kh Tohidul Islam⁵, Zhaolin Chen⁵, Zi Wang¹,
Peter Lally¹, and Guang Yang^{1,2,3,4}

- ¹ Department of Bioengineering and Imperial-X, Imperial College London, London, UK
{zz2524, peiyuan.jing22, r.yuan25, l.hu25, w.anbang25, fanwen.wang,
yinzhe.wu18, zi.wang, p.lally, g.yang}@imperial.ac.uk
- ² National Heart and Lung Institute, Imperial College London, London SW7 2AZ, U.K.
- ³ Cardiovascular Research Centre, Royal Brompton Hospital, London SW3 6NP, U.K.
- ⁴ School of Biomedical Engineering & Imaging Sciences, King's College London, London WC2R 2LS, U.K.
- ⁵ Department of Electrical and Computer Systems Engineering, Monash University, Melbourne, Australia
{khtohidul.islam, zhaolin.chen}@monash.edu

Abstract. Low-field to high-field MRI synthesis has emerged as a cost-effective strategy to enhance image quality under hardware and acquisition constraints, particularly in scenarios where access to high-field scanners is limited or impractical. Despite recent progress in diffusion models, diffusion-based approaches often struggle to balance fine-detail recovery and structural fidelity. In particular, the uncontrolled generation of high-resolution details in structurally ambiguous regions may introduce anatomically inconsistent patterns, such as spurious edges or artificial texture variations. These artifacts can bias downstream quantitative analysis. For example, they may cause inaccurate tissue boundary delineation or erroneous volumetric estimation, ultimately reducing clinical trust in synthesized images. These limitations highlight the need for generative models that are not only visually accurate but also spatially reliable and anatomically consistent. To address this issue, we propose a reliability-aware diffusion framework (ReDiff) that improves synthesis robustness at both the sampling and post-generation stages. Specifically, we introduce a reliability-guided sampling strategy to suppress unreliable responses during the denoising process. We further develop an uncertainty-aware multi-candidate selection scheme to enhance the reliability of the final prediction. Experiments on multi-center MRI datasets demonstrate improved structural fidelity and reduced artifacts compared with state-of-the-art methods.

Keywords: MRI Synthesis · Diffusion model · Image generation.

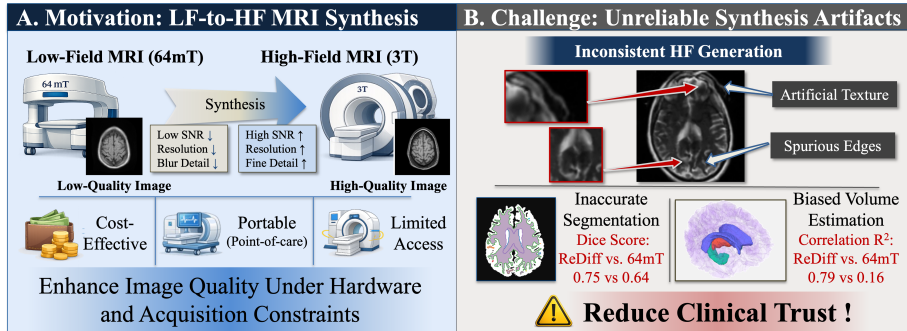


Fig. 1. Motivation and challenges of our Reliability-Guided Diffusion. (A) Low-field MRI (e.g., 64 mT) is cost-effective and accessible but typically produces lower-quality images. LF-to-HF synthesis seeks to recover high-field (e.g., 3T) image fidelity under hardware and acquisition constraints. (B) Despite recent progress, diffusion-based methods may introduce unreliable high-resolution artifacts, such as artificial textures and spurious edges. These errors can degrade downstream tasks, leading to inaccurate segmentation, biased volume estimation, and reduced clinical trust.

1 Introduction

High-field (HF) MRI systems (e.g., 3T) provide superior signal-to-noise ratio and improved depiction of fine anatomical structures, particularly along tissue boundaries and cortical folding patterns [1,4]. They are also more reliable in resolving low-contrast soft-tissue regions and small pathological variations. In contrast, low-field (LF) MRI (e.g., 64 mT) typically exhibits reduced spatial resolution, elevated noise levels, and blurred structural boundaries, with degradation being most pronounced in thin cortical regions, deep gray matter structures and other anatomically complex areas [1,15]. As a result, the quality gap between LF and HF imaging is highly spatially heterogeneous rather than uniform across the image [10,21]. Therefore, LF-to-HF MRI synthesis has emerged as a promising computational strategy to reduce this spatially heterogeneous quality gap and enhance structural fidelity without requiring hardware upgrades [14]. Importantly, for clinical adoption, synthesized images must be not only visually realistic but also anatomically faithful and quantitatively reliable.

Despite recent advances, low-field to high-field MRI synthesis remains challenged by the presence of unreliable synthesis artifacts [10,21,18,8,20,16]. These artifacts typically arise from uncontrolled generation during the reconstruction process and may manifest as spurious edges, artificial texture variations or anatomically implausible structural details [21,12]. Importantly, such errors are not uniformly distributed across the image but tend to concentrate in structurally ambiguous and anatomically complex regions, where the underlying signal is inherently uncertain [20,16]. This spatially heterogeneous behavior makes the artifacts particularly difficult to detect and correct. Even subtle structural inconsistencies may propagate to downstream analyses and impact clinical inter-

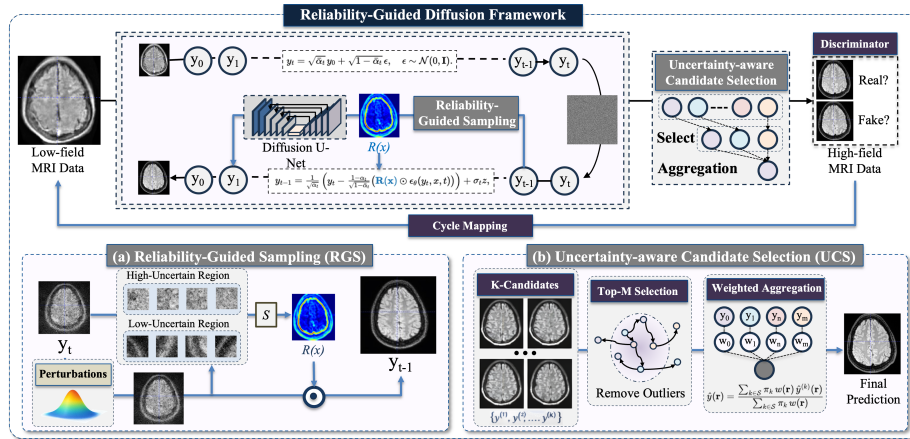


Fig. 2. Reliability-Guided Diffusion (ReDiff) framework for LF-to-HF MRI synthesis. Given a low-field (LF) image x , a conditional diffusion U-Net predicts the noise term $\epsilon_\theta(y_t, x, t)$ to iteratively recover the high-field (HF) image. (a) In the proposed reliability-guided sampling (RGS), a spatial reliability map $\mathbf{R}(x)$ modulates the reverse diffusion update to suppress unsupported high-frequency amplification in ill-posed regions. (b) To further enhance robustness, uncertainty-aware candidate selection (UCS) generates multiple candidates and performs reliability-weighted aggregation based on spatial uncertainty. Together, the two-stage design improves structural consistency while reducing hallucinated details in LF-to-HF synthesis.

pretation. For example, artificial boundary patterns can lead to inaccurate tissue delineation, while texture distortions may introduce bias in volumetric estimation. These effects ultimately undermine the reliability of synthesized images and raise concerns about their safe clinical use. These limitations highlight the need for generative models that explicitly account for spatially varying reconstruction reliability during the synthesis process.

Recent diffusion-based approaches have demonstrated strong capability in recovering high-resolution details and improving perceptual image quality for LF-to-HF MRI synthesis [9,13,22,23]. However, most existing methods primarily rely on globally uniform denoising objectives. As a result, they often lack explicit mechanisms to regulate spatially varying reconstruction reliability during the synthesis procedure [24,7]. In particular, the denoising process in standard diffusion frameworks treats all spatial locations and frequency components in a largely homogeneous manner, which may inadvertently amplify unreliable responses in structurally ambiguous regions. Although several studies have explored perceptual losses, adversarial learning, or multi-scale architectures to enhance visual fidelity, these strategies mainly focus on improving overall image realism rather than explicitly modeling where the generation process is trustworthy. Consequently, the problem of spatially inconsistent synthesis remains insufficiently addressed in current LF-to-HF MRI reconstruction pipelines.

To address these limitations, we propose a reliability-aware diffusion (ReDiff) framework that explicitly mitigates spatially inconsistent generation during diffusion. Our approach integrates two complementary strategies at different stages of the pipeline. First, a reliability-guided sampling mechanism dynamically suppresses unreliable high-frequency responses along the denoising trajectory, reducing the risk of amplifying spurious structures in ambiguous regions. Second, we enhance synthesis robustness via a post-generation candidate selection scheme, where multiple reconstructions are evaluated with an uncertainty-aware criterion and the most reliable prediction is selected or aggregated. This design provides an additional safeguard against spatial inconsistency. Extensive experiments on multi-center MRI datasets demonstrate improved structural fidelity and reduced high-frequency artifacts compared with state-of-the-art methods. Our contributions are summarized as follows:

1. We identify the problem of spatially unreliable high-frequency generation in LF-to-HF MRI synthesis and analyze its impact on structural fidelity.
2. We propose a reliability-aware diffusion framework that suppresses unreliable detail amplification during sampling and further improves robustness via uncertainty-aware candidate selection.
3. Extensive experiments on multi-center paired LF to HF MRI datasets demonstrate consistent improvements in structural fidelity and reliability over state-of-the-art methods.

2 Methodology

Problem Formulation Let $y \in \mathbb{R}^{H \times W \times D}$ denote the latent HF MRI volume acquired at main field strength B_H and $x \in \mathbb{R}^{H \times W \times D}$ the observed LF volume acquired at B_L ($B_L < B_H$). We model the LF image as a field-strength-dependent observation of the same underlying anatomy:

$$x = \mathcal{F}_{B_L}(y) + \epsilon_{B_L}, \quad \epsilon_{B_L} \sim \mathcal{N}(0, \sigma^2(B_L)\mathbf{I}), \quad (1)$$

where \mathcal{F}_{B_L} represents the effective low-field imaging operator that attenuates high-frequency information and modifies tissue contrast, and $\sigma^2(B_L)$ reflects the increased noise level associated with reduced B_0 . Due to the loss of high-frequency observability and elevated noise at low field, recovering y from x is intrinsically ill-posed. This uncertainty makes conditional generation prone to spatially unreliable high-frequency hallucinations in regions where the LF evidence is weak.

Diffusion-based approaches address this task by learning the conditional distribution $p_\theta(y | x)$ and generating \hat{y} via iterative denoising. However, in regions where \mathcal{F}_{B_L} severely attenuates high-frequency information, the posterior becomes highly uncertain, which may lead to over-amplified high-frequency responses and spatially inconsistent structures during sampling. To mitigate this issue, we aim to learn a reliability-aware generator

$$\hat{y} = \mathcal{G}(x; \theta) = \arg \max_y p_\theta(y | x) \mathcal{R}(y, x), \quad (2)$$

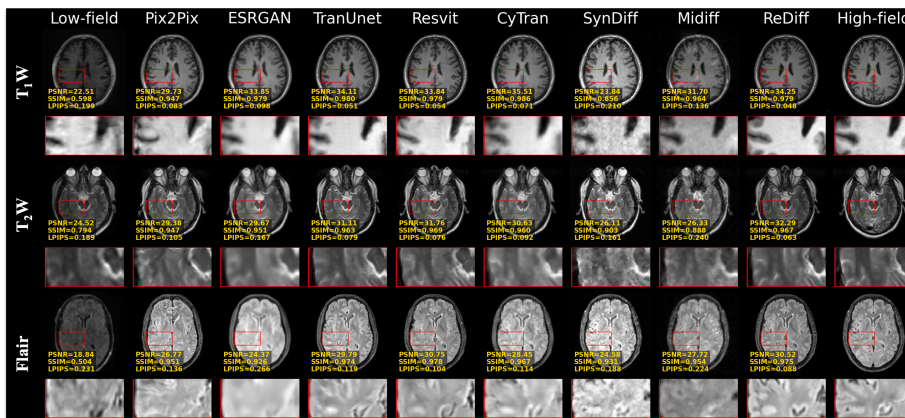


Fig. 3. Qualitative comparison of multi-contrast low-field to high-field MRI synthesis. For each case, the top row shows full images and the bottom row shows zoomed views of the red boxed regions. ReDiff produces sharper anatomical structures and fewer artifacts, with PSNR and SSIM reported on each result.

where $\mathcal{R}(y, x)$ denotes a spatial reliability prior that suppresses unsupported high-frequency generation while preserving anatomically consistent details.

Reliability-Guided Sampling (RGS) Diffusion-based conditional synthesis generates the HF image by iteratively denoising a noisy variable y_t towards y_0 . Following the standard formulation, the reverse diffusion step can be written as

$$y_{t-1} = \frac{1}{\sqrt{\alpha_t}} \left(y_t - \frac{1 - \alpha_t}{\sqrt{1 - \bar{\alpha}_t}} \epsilon_\theta(y_t, x, t) \right) + \sigma_t z, \quad z \sim \mathcal{N}(0, \mathbf{I}), \quad (3)$$

where $\epsilon_\theta(\cdot)$ denotes the predicted noise conditioned on the LF image x .

As discussed in Problem Formulation, low-field acquisition reduces the observability of high-frequency structures. In regions with weak LF evidence, the posterior uncertainty increases, and the standard reverse update may over-amplify high-frequency responses, leading to spatially inconsistent hallucinations.

To address this issue, we introduce a diffusion-aware spatial reliability map $R(x) \in [0, 1]^{H \times W \times D}$. Specifically, $R(x)$ is estimated from the local stability of the diffusion model under small perturbations of the noisy state. We approximate the local sensitivity by injecting Gaussian perturbations $\delta \sim \mathcal{N}(0, \sigma_p^2 I)$ to y_t and computing $S = \mathbb{E}_\delta [|\epsilon_\theta(y_t + \delta, x, t) - \epsilon_\theta(y_t, x, t)|]$, and define the reliability map as $R(x) = \exp(-\gamma S)$, where γ controls the attenuation strength. Regions with higher sensitivity are considered less reliable and assigned lower weights. The reverse update is therefore modulated in a spatially adaptive manner:

$$y_{t-1} = \frac{1}{\sqrt{\alpha_t}} \left(y_t - \frac{1 - \alpha_t}{\sqrt{1 - \bar{\alpha}_t}} (R(x) \odot \epsilon_\theta(y_t, x, t)) \right) + \sigma_t z, \quad (4)$$

Table 1. Evaluation on the paired 64mT→3T dataset under Multi-Contrast setting. * indicates $p < 0.05$ and ** indicates $p < 0.01$ in a Wilcoxon signed-rank test against our ReDiff model. **Bold** indicates the best result and underline indicates the second best.

Setting	Method	Year	Private Dataset			Leiden Uni. Dataset		
			PSNR↑	SSIM↑	LPIPS↓	PSNR↑	SSIM↑	LPIPS↓
T_{1w}	Low-field	-	24.83±2.77**	0.758±0.133**	0.2222±0.0866**	24.73±2.81**	0.768±0.117**	0.2138±0.0741**
	Pix2Pix[11]	2017	30.51±2.62**	0.933±0.052**	0.1050±0.0394**	30.71±2.64**	0.939±0.054**	0.1043±0.0366**
	ESRGAN[19]	2018	31.72±2.54**	0.949±0.038*	0.1080±0.0746**	32.08±2.46**	0.958±0.029	0.1034±0.0704**
	TranUnet[5]	2021	31.71±2.75**	0.939±0.092**	0.0947±0.0720*	32.08±2.72**	0.950±0.069*	0.0901±0.0592*
	ResViT[6]	2022	31.61±2.75**	0.941±0.058**	0.0887±0.0505*	32.10±2.65**	0.953±0.045*	0.0838±0.0435
	CyTran[17]	2023	32.76±2.78*	0.961±0.065	0.0950±0.0451*	<u>33.21±2.65</u>	0.970±0.047	0.0909±0.0389*
	SynDiff[16]	2023	33.34±2.36	0.953±0.003	0.1102±0.0361**	33.20±2.10	0.953±0.003	0.1174±0.0404**
	MiDiffusion[20]	2024	32.77±4.79*	0.944±0.053**	0.1717±0.0428**	32.54±4.78**	0.942±0.056**	0.1714±0.0410**
	ReDiff		<u>32.89±2.59</u>	<u>0.957±0.038</u>	0.0835±0.0590	33.39±2.69	<u>0.965±0.029</u>	0.0753±0.0389
	T_{2w}	Low-field	-	24.90±2.93**	0.753±0.132**	0.2192±0.0820**	25.01±2.94**	0.765±0.130**
Pix2Pix[11]		2017	30.64±2.71**	0.932±0.052**	0.1072±0.0381**	30.78±2.90**	0.936±0.051**	0.1049±0.0414**
ESRGAN[19]		2018	31.94±2.59**	0.950±0.040*	0.1069±0.0770**	32.22±2.66*	0.956±0.031	0.1050±0.0824**
TranUnet[5]		2021	31.83±2.78**	0.939±0.091**	0.0950±0.0705*	32.21±2.92*	0.945±0.098*	0.0932±0.0774*
ResViT[6]		2022	31.72±2.81**	0.939±0.065**	0.0899±0.0559*	32.14±2.92*	0.948±0.064*	0.0860±0.0576
CyTran[17]		2023	32.93±2.88*	0.963±0.049	0.0952±0.0455*	<u>33.23±3.01</u>	0.967±0.051	0.0962±0.0505*
SynDiff[16]		2023	33.17±2.39	0.952±0.004	0.1150±0.0399**	33.32±2.39	0.953±0.003	0.1148±0.0383**
MiDiffusion[20]		2024	32.11±4.83**	0.931±0.063**	0.1787±0.0438**	32.57±4.80*	0.940±0.059**	0.1740±0.0436**
ReDiff			<u>33.06±2.77</u>	<u>0.958±0.038</u>	0.0820±0.0486	33.22±2.85	<u>0.958±0.056</u>	0.0842±0.0574
Flair		Low-field	-	24.68±2.85**	0.758±0.115**	0.2238±0.0856**	24.98±2.95**	0.757±0.114**
	Pix2Pix[11]	2017	30.64±2.51**	0.937±0.040**	0.1079±0.0423**	30.97±2.61**	0.938±0.048**	0.1048±0.0334**
	ESRGAN[19]	2018	31.86±2.52**	0.953±0.034*	0.1139±0.0940**	32.08±2.75*	0.951±0.041*	0.1074±0.0759**
	TranUnet[5]	2021	31.88±2.71**	0.948±0.051*	0.0973±0.0745*	32.08±2.86*	0.945±0.057*	0.0943±0.0557*
	ResViT[6]	2022	31.94±2.68**	0.949±0.048*	0.0912±0.0750*	32.24±2.79*	0.949±0.045*	0.0865±0.0480
	CyTran[17]	2023	<u>33.05±2.72</u>	0.969±0.031	0.0996±0.0660*	33.31±2.94	0.966±0.046	0.0941±0.0424*
	SynDiff[16]	2023	32.96±2.12	0.953±0.005	0.1169±0.0420**	33.13±2.35	0.953±0.003	0.1178±0.0385**
	MiDiffusion[20]	2024	32.23±4.66**	0.936±0.061**	0.1792±0.0578**	32.62±4.62*	0.939±0.057**	0.1773±0.0435**
	ReDiff		33.06±2.61	<u>0.960±0.039</u>	0.0859±0.0698	<u>33.30±2.77</u>	<u>0.960±0.037</u>	0.0821±0.0478

where \odot denotes element-wise multiplication. This modulation suppresses unstable updates in ill-posed regions while preserving standard diffusion behavior in reliable areas, thereby improving structural consistency and reducing hallucinated details.

Uncertainty-aware Candidate Selection (UCS) While the proposed reliability-guided sampling reduces the risk of unreliable updates during generation, residual uncertainty may still remain due to the intrinsic ill-posedness of LF-to-HF synthesis. To further improve robustness, we introduce an uncertainty-aware candidate selection scheme as a complementary post-generation safeguard.

Given the LF input x , we generate K candidate HF reconstructions by stochastic diffusion sampling:

$$\{\hat{y}^{(k)}\}_{k=1}^K \sim p_{\theta}(y | x). \quad (5)$$

These candidates reflect the posterior variability induced by noise and ambiguous LF evidence.

To suppress structurally inconsistent samples, we first measure the similarity of each candidate to the consensus. Let $\mu(r) = \frac{1}{K} \sum_{k=1}^K \hat{y}^{(k)}(r)$ denote the candidate mean. We compute a deviation score $d^{(k)}(\mathbf{r}) = |\hat{y}^{(k)}(\mathbf{r}) - \mu(\mathbf{r})|$. Candidates with large deviations are regarded as potential outliers. We retain the top- M most consistent candidates according to the spatially averaged deviation score and discard the rest. On the filtered candidate set, we estimate spatial

Table 2. Ablation study of the proposed ReDiff framework on the Private and Leiden datasets. RGS denotes reliability-guided sampling and UCS denotes uncertainty-aware candidate selection. Bold indicates the full model.

RGS UCS		Private Dataset			Leiden Uni. Dataset		
		PSNR \uparrow	SSIM \uparrow	LPIPS \downarrow	PSNR \uparrow	SSIM \uparrow	LPIPS \downarrow
×	×	30.98 \pm 2.55	0.934 \pm 0.060	0.1080 \pm 0.0697	31.32 \pm 2.63	0.940 \pm 0.054	0.1038 \pm 0.0628
✓	×	31.72 \pm 2.51	0.945 \pm 0.052	0.1062 \pm 0.0717	32.11 \pm 2.67	0.950 \pm 0.049	0.1022 \pm 0.0622
×	✓	31.45 \pm 2.60	0.940 \pm 0.056	0.0991 \pm 0.0687	31.82 \pm 2.73	0.946 \pm 0.057	0.0946 \pm 0.0587
✓	✓	33.00\pm2.66	0.959\pm0.038	0.0838\pm0.0595	33.30\pm2.77	0.961\pm0.043	0.0806\pm0.0490

uncertainty via the empirical variance:

$$U(\mathbf{r}) = \text{Var}(\{\hat{y}^{(k)}(\mathbf{r})\}). \quad (6)$$

The final reconstruction is obtained by reliability-weighted aggregation:

$$\hat{y}(\mathbf{r}) = \frac{\sum_k w^{(k)}(\mathbf{r}) \hat{y}^{(k)}(\mathbf{r})}{\sum_k w^{(k)}(\mathbf{r})}, \quad w^{(k)}(\mathbf{r}) = \exp\left(-\beta U(\mathbf{r}) d^{(k)}(\mathbf{r})\right), \quad (7)$$

where β controls the strength of uncertainty suppression. This process effectively suppresses unsupported hallucinations while preserving anatomically consistent structures.

Training Objective. The network is trained under the standard diffusion objective together with reconstruction and adversarial regularizations to encourage structural fidelity and perceptual realism. The overall loss is defined as

$$\mathcal{L} = \lambda_1 \|\hat{y} - y\|_1 + \lambda_2 (1 - \text{SSIM}(\hat{y}, y)) + \lambda_3 \mathcal{L}_{\text{adv}} + \lambda_4 \mathcal{L}_{\text{cyc}}, \quad (8)$$

where \hat{y} and y denote the synthesized and ground-truth HF images, respectively. The first two terms enforce pixel-wise accuracy and structural consistency. \mathcal{L}_{adv} denotes the adversarial loss that encourages realistic high-frequency details, and \mathcal{L}_{cyc} represents the cycle-consistency loss that regularizes cross-domain mapping stability. The hyperparameters λ_1 – λ_4 balance different objectives.

3 Experiments

Datasets. We evaluate the proposed ReDiff framework on three paired LF–HF MRI datasets. The first is a private dataset containing 20 subjects with T₁w, T₂w, and FLAIR scans acquired at both 64mT and 3T. The second is the publicly available Leiden dataset with 11 healthy subjects scanned at both field strengths, including localizer, T₁w, T₂w, and FLAIR sequences [3].

Implementation Details. The proposed ReDiff is optimized using Adam with an initial learning rate of 2×10^{-3} . The diffusion model uses 1000 timesteps with a linear noise schedule. All experiments are conducted on a workstation equipped with NVIDIA H200 GPU. We report PSNR and SSIM to measure intensity fidelity and structural similarity, respectively, and LPIPS to evaluate perceptual consistency in feature space.

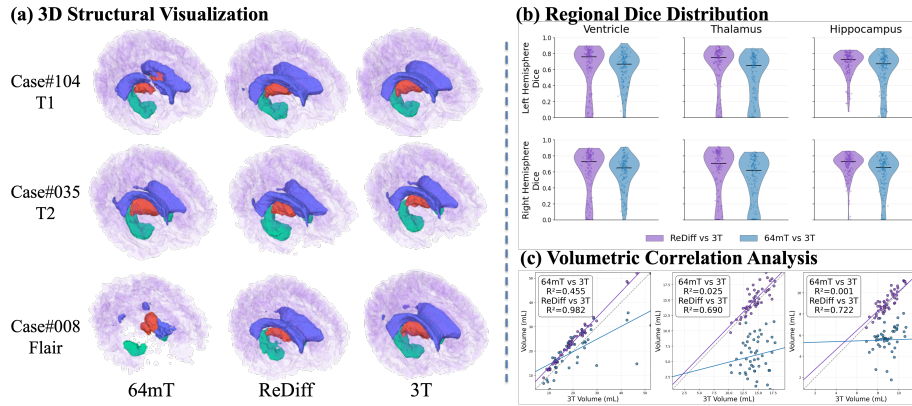


Fig. 4. Qualitative and quantitative downstream validation. (a) 3D structural visualization of SynthSeg-derived segmentations for representative cases. (b) Regional Dice distributions for the ventricle, thalamus, and hippocampus in both hemispheres. (c) Volumetric correlation with respect to the 3T reference.

Comparison Experiment. Table 1 quantitatively compares different methods on the paired 64mT→3T dataset. Overall, diffusion-based baselines achieve competitive PSNR in several cases and CyTran attains the highest SSIM on some contrasts. In contrast, the proposed ReDiff consistently yields the lowest LPIPS across all three contrasts and both datasets, suggesting improved perceptual fidelity. The visual comparisons in Fig. 3 further support these findings. As highlighted in the zoomed regions, Low-field and early GAN-based methods exhibit noticeable blurring and loss of cortical details. Recent diffusion-based model (e.g., SynDiff) tends to introduce over-smoothed or noisy textures, particularly in T₁w and FLAIR. ReDiff produces sharper tissue boundaries and more faithful fine-grained patterns that better match the high-field reference.

Ablation Study. Table 2 evaluates the effects of the RGS and UCS modules. RGS alone brings consistent improvement (31.72 dB), indicating the benefit of reliability-aware modulation during diffusion sampling. UCS also yields clear gains, improving PSNR to 31.45 dB and reducing LPIPS from 0.1080 to 0.0991 on private dataset, with similar trends observed on the Leiden dataset. Combining both modules achieves the best performance, demonstrating their complementary roles in enhancing structural fidelity and robustness.

Downstream Qualitative Validation. Fig.4 presents downstream evaluation based on SynthSeg-derived segmentations [2]. In Fig.4(a), representative neuroanatomical structures are rendered as 3D meshes. ReDiff produces clearer boundaries and more anatomically coherent morphology than the low-field baseline. Quantitative distributions in Fig.4(b) show consistently higher Dice scores across regions and hemispheres. Furthermore, the volumetric correlation in Fig.4(c) demonstrates substantially improved agreement with the 3T

reference. These results indicate that ReDiff better preserves structurally and volumetrically meaningful information for downstream analysis.

4 Conclusion

In this work, we propose a reliability-aware diffusion (ReDiff) framework for low-field to high-field MRI synthesis. ReDiff models reliability in both sampling and post-generation, suppressing unstable denoising responses and improving robustness via uncertainty-aware candidate selection. Experiments on multi-center MRI datasets demonstrate improved structural fidelity and reduced artifacts over state-of-the-art methods. Future work will explore tighter integration with downstream tasks and broader cross-modality and low-SNR scenarios.

5 Acknowledgment

Guang Yang was supported in part by the ERC IMI (101005122), the H2020 (952172), the MRC (MC/PC/21013), the Royal Society (IEC/NSFC/211235), the NVIDIA Academic Hardware Grant Program, the SABER project supported by Boehringer Ingelheim Ltd, NIHR Imperial Biomedical Research Centre (RDA01), The Wellcome Leap Dynamic resilience program (co-funded by Temasek Trust), UKRI guarantee funding for Horizon Europe MSCA Postdoctoral Fellowships (EP/Z002206/1), UKRI MRC Research Grant, TFS Research Grants (MR/U506710/1), Swiss National Science Foundation (Grant No. 220785), and the UKRI Future Leaders Fellowship (MR/V023799/1). Zhenxuan Zhang was supported by a CSC Scholarship.

References

1. Arnold, T.C., Freeman, C.W., Litt, B., Stein, J.M.: Low-field MRI: Clinical promise and challenges. *Journal of Magnetic Resonance Imaging* **57**(1), 25–44 (Sep 2022). <https://doi.org/10.1002/jmri.28408>
2. Billot, B., Greve, D.N., Puonti, O., Thielscher, A., Van Leemput, K., Fischl, B., Dalca, A.V., Iglesias, J.E.: Synthseg: Segmentation of brain mri scans of any contrast and resolution without retraining. *Medical Image Analysis* **86**, 102789 (May 2023). <https://doi.org/10.1016/j.media.2023.102789>
3. van den Broek, R., Lena, B., Webb, A.: Paired 64mT and 3T Brain MRI Scans of Healthy Subjects for Neuroimaging Research (2024). <https://doi.org/10.5281/ZENODO.15862148>
4. Brown, R.W., Cheng, Y.C.N., Haacke, E.M., Thompson, M.R., Venkatesan, R., Cheng, Y.C.N.: *Magnetic Resonance Imaging: Physical Principles and Sequence Design*. Wiley, Newark, NJ, 2nd edn. (2014)
5. Chen, J., Mei, J., Li, X., et al.: TransUNet: Rethinking the U-Net architecture design for medical image segmentation through the lens of transformers. *Medical Image Analysis* **97**, 103280 (Oct 2024). <https://doi.org/10.1016/j.media.2024.103280>

6. Dalmaz, O., Yurt, M., Cukur, T.: ResViT: Residual Vision Transformers for Multimodal Medical Image Synthesis. *IEEE Transactions on Medical Imaging* **41**(10), 2598–2614 (Oct 2022). <https://doi.org/10.1109/TMI.2022.3167808>
7. Dayarathna, S., Peiris, H., Islam, K.T., Wong, T.T., Chen, Z.: D2Diff: A Dual-Domain Diffusion Model for Accurate Multi-Contrast MRI Synthesis, p. 131–141. Springer Nature Switzerland (Sep 2025). https://doi.org/10.1007/978-3-032-04937-7_13
8. Ding, Y., Vardhanabhuti, V., Huang, F., Xiao, L., Su, S., Hu, J., Zhang, J., Lau, V., Man, C., Zhao, Y., Leong, A.T.L., Wu, E.X.: Ultra-low-field balanced steady-state free precession mri at 0.05 tesla. *IEEE Transactions on Biomedical Engineering* **73**(1), 245–254 (Jan 2026). <https://doi.org/10.1109/tbme.2025.3580111>
9. Ho, J., Jain, A., Abbeel, P.: Denoising diffusion probabilistic models. NIPS '20, Curran Associates Inc., Red Hook, NY, USA (2020)
10. Islam, K.T., Ekanayake, M., Chen, Z.: Ultra-Low-Field MRI Enhancement via INR-Based Style Transfer, p. 597–607. Springer Nature Switzerland (Sep 2025). https://doi.org/10.1007/978-3-032-05325-1_57
11. Isola, P., Zhu, J.Y., Zhou, T., Efros, A.A.: Image-to-Image Translation with Conditional Adversarial Networks. In: 2017 IEEE Conference on Computer Vision and Pattern Recognition (CVPR). pp. 5967–5976. IEEE, Honolulu, HI (Jul 2017). <https://doi.org/10.1109/CVPR.2017.632>
12. Javadi, M., Griffin, R., Tsiamyrtzis, P., Leiss, E., Webb, A.G., Tsekos, N.V.: In-silico comparison of a diffusion model with conventionally trained deep networks for translating 64mt to 3t brain flair. *Scientific Reports* **15**(1) (Oct 2025). <https://doi.org/10.1038/s41598-025-21806-9>
13. Liu, H., Xue, W., Chen, Y., Chen, D., Zhao, X., Wang, K., Hou, L., Li, R., Peng, W.: A Survey on Hallucination in Large Vision-Language Models (2024). <https://doi.org/10.48550/ARXIV.2402.00253>
14. Man, C., Lau, V., Su, S., Zhao, Y., Xiao, L., Ding, Y., Leung, G.K.K., Leong, A.T.L., Wu, E.X.: Deep learning enabled fast 3d brain mri at 0.055 tesla. *Science Advances* **9**(38) (Sep 2023). <https://doi.org/10.1126/sciadv.adi9327>
15. Mazurek, M.H., Cahn, B.A., Yuen, M.M., et al.: Portable, bedside, low-field magnetic resonance imaging for evaluation of intracerebral hemorrhage. *Nature Communications* **12**(1), 5119 (Aug 2021). <https://doi.org/10.1038/s41467-021-25441-6>
16. Özbey, M., Dalmaz, O., Dar, S.U., Bedel, H.A., Öztürk, Ş., Güngör, A., Cukur, T.: Unsupervised Medical Image Translation With Adversarial Diffusion Models. *IEEE Transactions on Medical Imaging* **42**(12), 3524–3539 (Dec 2023). <https://doi.org/10.1109/TMI.2023.3290149>
17. Ristea, N.C., Miron, A.I., Savencu, O., Georgescu, M.I., Verga, N., Khan, F.S., Ionescu, R.T.: CyTran: A cycle-consistent transformer with multi-level consistency for non-contrast to contrast CT translation. *Neurocomputing* **538**, 126211 (Jun 2023). <https://doi.org/10.1016/j.neucom.2023.03.072>
18. Su, S., Zhao, Y., Ding, Y., Lau, V., Xiao, L., Leung, G.K.K., Lau, G.K.K., Huang, F., Vardhanabhuti, V., Leong, A.T.L., Wu, E.X.: Ultra-low-field magnetization transfer imaging at 0.055t with low specific absorption rate. *Magnetic Resonance in Medicine* (Jul 2024). <https://doi.org/10.1002/mrm.30231>
19. Wang, X., Yu, K., Wu, S., Gu, J., Liu, Y., Dong, C., Qiao, Y., Loy, C.C.: ESRGAN: Enhanced Super-Resolution Generative Adversarial Networks. In: Computer Vision – ECCV 2018 Workshops: Munich, Germany, September 8–14, 2018, Proceedings, Part V. p. 63–79. Springer-Verlag, Berlin, Heidelberg (2018). https://doi.org/10.1007/978-3-030-11021-5_5

20. Wang, Z., Yang, Y., Chen, Y., Yuan, T., Sermesant, M., Delingette, H., Wu, O.: Mutual Information Guided Diffusion for Zero-Shot Cross-Modality Medical Image Translation. *IEEE Transactions on Medical Imaging* **43**(8), 2825–2838 (Aug 2024). <https://doi.org/10.1109/TMI.2024.3382043>
21. Yang, H., Liu, S., Liu, Y., Zhang, L., Huang, S., Zheng, J., Liu, J., Guo, H., Wu, E.X., Lyu, M.: An unsupervised learning approach for reconstructing 3t-like images from 0.3t mri without paired training data. *IEEE Transactions on Medical Imaging* **44**(12), 5358–5371 (Dec 2025). <https://doi.org/10.1109/tmi.2025.3597401>
22. Zhang, Z., Jing, P., Beitone, C., Huang, J., Gao, Z., Yang, G., Lally, P.: Pretext Task Adversarial Learning for Unpaired Low-field to Ultra High-field MRI Synthesis (Mar 2025). <https://doi.org/10.48550/arXiv.2503.05339>
23. Zhang, Z., Jing, P., Wang, Z., et al.: Cyclic Self-Supervised Diffusion for Ultra Low-field to High-field MRI Synthesis (Oct 2025). <https://doi.org/10.48550/arXiv.2510.13735>
24. Zhang, Z., Zhang, L., Cheng, Y., et al.: From Coarse to Continuous: Progressive Refinement Implicit Neural Representation for Motion-Robust Anisotropic MRI Reconstruction (Jun 2025). <https://doi.org/10.48550/arXiv.2506.16210>